
Check for updates

where x and γ are the mole fraction and the activity coefficient of $RaSO_4$, respectively. Consequently,

$$a(Ra^{2+}) = K_S x\gamma / a(SO_4^{2+}). \quad (2)$$

Here we mention that throughout the text $RaSO_4$ should be understood as ether a component of a solid solution or as a pure solid $RaSO_4$ phase. The latter distinction is always made clear from the context. Therefore, the index *s*, e.g. in $RaSO_4$,s, is avoided for brevity. Eqn. (2) shows that the formation of a dilute ideal ($\gamma = 1$) solid solution with $x = 0.001$ would decrease the aqueous activity of Ra by three orders of magnitude. For this reason, the dilution in a solid solution with barite can efficiently retard aqueous migration of radium. Hence, the demonstration of thermodynamic stability of barite minerals within engineered and geological barriers becomes an important item for safety assessments. It is often assumed that even if primary barite is absent in the host rock, a certain amount of secondary barite could be formed at the contamination front due to the release of Ba that is contained within the nuclear waste (Grandia et al., 2008) and the sulphate contained in the ground water. It is likely that the formation of this secondary barite will precede a significant release of Ra. Indeed, the ^{226}Ra escape will be controlled by isotope equilibria with actinides, and thus will persist over a long time interval, while the escape of Ba, which is presumably contained in the spent fuel as oxide precipitates (Bruno and Ewing, 2006), will probably occur soon after the container failure.

Although a large portion of the released Ra could be taken up by secondary barite, its sorption capacity would likely be small compared to the capacity of Sr-containing sulphates present in a host rock. As natural alkali-earth sulfates typically form $(Ba,Sr)SO_4$ solid solutions (Hanor, 2000), a theoretical demonstration of the efficiency of Ra retention by natural sulfates requires a thermodynamic description of the ternary $(Ba,Sr,Ra)SO_4$ system. In prospective host rocks, such as the Opalinus clay formation (Switzerland) several generations of barite-type minerals has been described (Lerouge et al., 2014). The earlier generations, formed presumably during the burial stage of sedimentation, are represented by barite-rich solid solutions of a wide range of compositions, which typically occur among other diagenetic minerals filling out pores in bioclasts. The latest generation, formed predominantly along fault zones, is represented by celestite-rich varieties. In the Callovo-Oxfordian argillite at Bure (France), sulfates are mostly represented by celestites that contain from 7 to 16% of $BaSO_4$, (Lerouge et al., 2011). These and other observations show that pure $BaSO_4$ barite never occurs in natural clay rocks, thus the Ra sorption capacity should be assessed as a function of the celestite content.

Eqn. (2) shows that the effect of dilution is counterbalanced by the effect of non-ideal mixing, which is expressed by the value of γ. Our previous study (Vinograd et al., 2013) has allowed us to put constraints onto the value γ in the binary $(Ba,Ra)SO_4$ system. Our atomistic simulations showed that the mixing in this system is characterized by very small degree of non-ideality ($\gamma \approx 3$), and consequ
uptake by a pure $BaSO_4$ barite is very eff
qualitative arguments su
Ba ratio. It can be assum
Ra^{2+} and Sr^{2+}, the mix
very limited. Conseque
negative effect on Ra
tite, and, conceivably
the aqueous phase w
keep Ra^{2+} in the sol
can only be assesse

(2000) for a detailed review
$(Ba,Sr)SO_4$ compositions at ambient conditions, it was inferred that this solid solution is thermodynamically ideal (e.g. Brower and Renault, 1971). On the other hand, Galinier et al. (1989), based on dissolution experiments, argued for a moderate degree of non-ideality, which is equivalent to a positive regular model interaction parameter W_{BaSr} of 4.0 ± 0.3 kJ/mol. Similar estimates of 4.5–6.2 kJ/mol were derived from energy-volume relationships by Malinin and Urusov (1983). More recently, Becker et al. (2000), using the force-field model of Allan et al. (1993), arrived at a significantly larger effective W_{BaSr} value of ~8.3 kJ/mol. Zhu (2004), using an energy vs. volume correlation and available estimates of W values from co-precipitation experiments for various host-trace barite-type pairs, arrived at a value of W_{BaSr} of about 3.8 kJ/mol. The same study allowed the estimation of the mixing parameters in other binaries: W values of ~1.2 and ~8.1 kJ/mol for $(Ba,Ra)SO_4$ and $(Sr,Ra)SO_4$, respectively, were obtained. Vinograd et al. (2013), based on ab initio calculated defect formation energies, arrived at W values of ~2.5, ~8.4, and ~19.9 for $(Ba,Ra)SO_4$, $(Ba,Sr)SO_4$ and $(Sr,Ra)SO_4$, respectively.

The last set of parameters is further refined in the present study. Complementing the previous study, we make a consistent attempt to take into account effects of short-range and long-range ordering (SRO and LRO). Here we show that magnitudes of the pairwise interactions, which are responsible for the SRO and LRO, in the binary systems of $(Ba,Ra)SO_4$, $(Ba,Sr)SO_4$ and $(Sr,Ra)SO_4$ are proportional to the magnitudes of the W parameters. Modelling of the effects of ordering is performed here within the frame of the generalized Ising model. We find that the mixing properties within the $(Ba,Sr)SO_4$ binary are especially sensitive to the effect of SRO. Including this effect into models helps to partially resolve the controversy regarding the values of W_{BaSr} parameters reported in the literature.

The aim of this study is threefold. First, we evaluate a consistent set of the mixing parameters for $(Ba,Sr,Ra)SO_4$. Second, with the aid of the GEM-Selektor modelling package (http://gems.web.psi.ch), we apply this model to simulate certain scenarios relevant for the retention of Ra by rocks containing barite minerals with variable Sr/Ba ratios at ambient temperature. An extension to elevated temperatures is described in a companion paper (Vinograd et al., 2017). One of these scenario
predicts that an equilibration of a Sr-rich $(Ba,Sr)SO_4$ solid solutio
an aqueous Ra-bearing solution may lead to a nucleatio
phase, which is simultaneously rich in Ba and Ra. Th
experimental approach to test the model pr
equilibrate a powder of celestite that
Ra-bearing aqueous solution
formed Ra-rich crystal

2. M

short- or long-range order typically become important. An adequate description of these effects becomes possible with the generalized Ising model. This model requires the evaluation of the so-called pair interaction parameters, $J_{AB(n)}$, which operate at specific interatomic distances. These parameters can be evaluated only via an atomistic model.

As shown below, the W_{AB} and $J_{AB(n)}$ parameters can be computed from excess enthalpies of supercells containing single and paired substitutional defects. In this study these calculations are performed with $2 \times 2 \times 2$ supercells of barite with the compositions of $AB_{31}(SO_4)_{32}$ and $A_2B_{30}(SO_4)_{32}$, where A = Ba,Sr,Ra; B = Ba,Sr,Ra; $A \neq B$. In such a supercell, a single defect can be placed in any of the 32 equivalent positions, while a pair of defects can be inserted in 17 variants defined by the defect-defect distance. Thus, the derivation of W_{AB} requires a single geometry optimization (energy minimization) calculation, while the derivation of all $J_{AB(n)}$ parameters requires a larger computational effort. Here, the W_{AB} and $J_{AB(n)}$ parameters are evaluated both ab initio and with an empirically parameterized force-field model. The ab-initio total energies required for these evaluation were computed with the density functional theory (DFT) package CASTEP (Clark et al., 2005) using the Wu-Cohen density functional (Wu and Cohen, 2006). These calculations included optimizations of the electronic degrees of freedom, the atomic coordinates and unit-cell parameters. In all calculations the kinetic energy cutoff of the plane wave basis set was set at 1100 eV. The average distance between individual k-points was ~ 0.03 Å^{-1}. The effects of the core electrons on the wave functions of valence electrons were modelled with the ultrasoft on-the-fly-generated pseudopotentials supplied with the Materials Studio 7 software package [http://accelrys.com/products/collaborative-science/biovia-materials-studio]. Each geometry optimization required about 20000 CPU hours on the JuRoPa or JuReCa clusters at the Juelich Supercomputing Centre. The force-field static lattice energy minimization calculations were performed with the program GULP (Gale and Rohl, 2003). A geometry optimization task with GULP required about 0.5 min for each supercell on a single CPU. The calculations were performed with an empirical force-field model of Allan et al. (1993). The modifications relative to the original set of Allan et al. (1993) consisted in the parameterization of the Buckingham Ba – O interaction potential, $A \exp(-r/\rho)$, which was slightly adjusted to fit the unit cell parameters of barite from the study of Jacobsen et al. (1998). The new values are A = 4131.96028 eV and ρ = 0.290612 Å. Additionally, the Ra – O interaction potential with the parameters A = 3835.82299 eV and ρ = 0.299836 Å was introduced. The values for Ra – O were obtained by fitting to unit cell parameters of $RaSO_4$ from the study of Weigel and Trinkl (1973).

Below the binary regular mixing and the generalized Ising models are discussed in further details. The generalization of the binary models into their ternary variants follows this discussion.

2.1.1. Regular mixing model

In an (A,B)L solid solution in the dilute li
of a single substitutional
mation of Z_n pairs of A
where Z_n is the coordi
defect. The contributio
of each AB pair is equ
AA + BB = 2AB, w
pairwise interaction,
rounded by Z_n A ato
of mixing per 1 mol

atoms remains perfectly
next to a given B atom reduces from 1 to x_A. Thus, Eqn. (3) is modified as follows

$$H_{mix}(\text{regular}) = x_A x_B W_{AB}. \quad (4)$$

The last equation is consistent with the regular mixing model (Hildebrand, 1929). The W_{AB} parameter contains the total effect of the pairwise interactions at all distances. Their particular values are not important at this level of theory. We note, however, that typically the $J_{AB(n)}$ values vary with the composition. Under the assumption that this variation is linear

$$J_{AB(n)} = J_{AB/A(n)} x_A + J_{AB/B(n)} x_B, \quad (5)$$

where the values of $J_{AB/A(n)}$ and $J_{AB/B(n)}$ are defined in the limits of pure AL and BL, respectively, Eqn. (4) transforms into the subregular form

$$H_{mix}(\text{subregular}) = x_A x_B (x_A W_{AB/B} + x_B W_{AB/A}). \quad (6)$$

The values of $W_{AB/A}$ and $W_{AB/B}$ are evaluated here with the Single Defect Method (SDM) (Sluiter and Kawazoe, 2002). The SDM is based on noting that $W_{AB/A}$ and $W_{AB/B}$ are equal to the slopes of the enthalpy of mixing function (Eqn. (6)) in the vicinity of pure phases AL and BL. The slopes can be computed as the ratios of finite changes in the excess enthalpy and in the composition of a supercell of the host phase due to an insertion of a single substitutional defect corresponding to the other end member. The change in the mole fraction is given by the defect/host ratio, i.e. by the inverse of the number of the exchangeable sites, m, in the supercell. Therefore,

$$W_{AB/A} \approx \left.\frac{dH_{mix}}{dx_B}\right|_{x_B=0} \approx \frac{\Delta H_{mix}(\text{at } x_B = 1/m)}{1/m} = \Delta H_B. \quad (7)$$

Similarly, $W_{AB/B} = \Delta H_A$. In this study m = 32.

Although the obtained parameters are valid only in the dilute limits, they usually perform well in the high-temperature limit too. This can be verified by computing directly the excess energy of a supercell, in which the distribution of A and B is randomized. A supercell with a nearly perfectly random distribution can be emulated with the help of a special quasi-random structure (QRS). A QRS is an ordered structure (i.e. a supercell with a certain A,B arrangement over the m sites) with well
defined cluster frequencies (Zunger et al., 1990), whose enthal
vides the best estimate of the average enthalpy of a disorde
Here such a QRS has been chosen from a large set of
supercell structures according to the criteri
quencies of AB-type pairs at each dista
deviate negligibly from $^1/_2 x_A x_$
$(W_{AB/A} + W_{AB/B})/2$ i
structure wit
mol

$x_A x_B$ value, while if $J_{AB(n)}$ is positive, $p_{AB(n)}$ will decrease. These deviations are typically magnified at $x_B = 0.5$, where the relative fractions of AB pairs increase. As these deviations are counterbalanced by the entropy factor, $p_{AB(n)}$ are also functions of the temperature. To allow for a variation in $p_{AB(n)}$, the enthalpy of mixing is modelled with the equation

$$H_{mix}(\text{Ising}) = \frac{1}{2}\sum_{n=1}^{N} p_{AB(n)} Z_n J_{AB(n)}. \tag{8}$$

If the $J_{AB(n)}$ are known, the values of $p_{AB(n)}$ and H_{mix} can be determined with the Monte Carlo method (e.g. Warren et al., 2001).

A computationally convenient algorithm for the determination of J_n is offered by the Double Defect Method (DDM) (e.g. Hoshino et al. (1993), Vinograd et al. (2009, 2010), Liu et al. (2016)). It has been shown that a $J_{AB(n)}$ is a function of the excess enthalpy of a supercell structure prepared from an end-member A*R* by the insertion of a pair of B defects at the *n*-th distance from each other. Namely,

$$J_{AB/A(n)} = (2\Delta H_B - \Delta H_{BB(n)})/D_n \tag{9}$$

where D_n is the degeneracy factor, which counts the number of BB pairs created per single B defect due to the periodic boundary conditions applied to the supercell. This number is typically 1 for pairs located at short distances, however, it takes larger integer values ($1 \le D_n \le Z_n$) for pairs whose distances approach half of the body diagonal of the supercell. The D_n and Z_n values for a $2 \times 2 \times 2$ supercell are given in Table A1 in Appendix A3. The pairwise interactions in the B-rich limit are computed similarly via

$$J_{AB/B(n)} = (2\Delta H_A - \Delta H_{AA(n)})/D_n \tag{10}$$

where ΔH_A and $\Delta H_{AA(n)}$ are the excess enthalpies of supercell structures of the host B with single, A-type, and double, AA-type, substitutional defects. Importantly, ΔH_B and ΔH_A must satisfy

$$\Delta H_B = W_{AB/A} = \frac{1}{2}\sum_{n=1}^{N} Z_n J_{AB/A(n)} = \frac{1}{2}\sum_{n=1}^{N} Z_n (2\Delta H_B - \Delta H_{BB(n)})/D_n \tag{11}$$

and

$$\Delta H_A = W_{AB/B} = \frac{1}{2}\sum_{n=1}^{N} Z_n J_{AB/B(n)} = \frac{1}{2}\sum_{n=1}^{N} Z_n (2\Delta H_A - \Delta H_{AA(n)})/D_n. \tag{12}$$

Eqns. (11) and (12) are often slightly violated due to computational inaccuracies, but the equalities can always be restored via slight adjustments in the values of ΔH_B and ΔH_A. These adjusted values are actually used to compute the pairwise interactions via Eqns. (9) and (10), thus ensuring consistency between the $J_{AB/(n)}$ and W_{AB} parameters. This consistency means that the enthalpy of mixing computed with Eqn. (8) would converge to the subregular mixing model when the pairwise probabilities approach the value of $x_A x_B$. This behavi
seen in Monte Carlo results obtained at a very high

2.1.3. Modelling of mixin

The regular mixing
ternary system via the
2001)

$$H_{mix} = \sum_{I\neq J}^{N} x_I x_J W_{IJ} + x$$

where W_{IJ} are the bi

$$S_{mix} = -R\sum_{I}$$

while the ternary Gibbs energy of mixing is computed as

$$G_{mix} = H_{mix} - TS_{mix}. \tag{15}$$

2.1.4. The ternary Ising model

The generalized Ising model can be extended to the ternary system as follows

$$H_{mix} = \frac{1}{2}\sum_{I\neq J}\sum_{n=1}^{N} p_{IJ(n)} Z_n J_{IJ(n)}, \tag{16}$$

where the first summation is over the three different types of pairs, AB, AC, and BC. The problem is that the dependence of $J_{IJ(n)}$ on the ternary composition should be specified. As the first approximation, a linear dependence of $J_{IJ(n)}$ on the ternary mole fractions can be assumed:

$$J_{IJ(n)} = J_{IJ/I(n)} x_I + J_{IJ/J(n)} x_J + J_{IJ/K(n)} x_K \tag{17}$$

The first two summands in Eqn. (17) contain the familiar binary $J_{IJ(n)}$ parameters, which are computed with the DDM. The last term defines the dependence of the $J_{IJ(n)}$ on the third component *K*. This parameter can be computed with a ternary variant of the DDM (Vinograd et al., 2010), in which the excess effects are computed for IJ-, II- and JJ-type double-defect structures inserted into a supercell of pure K*R* composition. Our ab initio calculations along this approach were not fully successful, resulting in unreasonably large fluctuations in the values $J_{IJ/K(n)}$. However, our force-field calculations, suggested that the $J_{IJ/K(n)}$ interactions can be reasonably accurately predicted with the approximation

$$J_{IJ/K(n)} = (J_{IJ/I(n)} x_I + J_{IJ/J(n)} x_J)/(x_I + x_J), \tag{18}$$

This approximation is further used in this study. Eqn. (18) can be shown to be consistent with Eqn. (13) under the assumption of $W_{IJK} = 0$. On the contrary, a deviation from Eqn. (18) would imply the existence of specific ternary interactions. A good performance of Eqn. (13) in predicting the enthalpies of ternary QRS under the condition of $W_{IJK} = 0$ (see Appendix A2) can be viewed as a proof for the validity of the approximation implied in Eqn. (18).

2.1.5. Calculation of free energies of mixing

The excess energy of a supercell structure
of A, B and C cations can be comput
probabilities of AB, AC and BC
occurrence frequencie
modelled her
in

pairwise [illegible] W_{mix} corresponds to the [illegible] of the binary or ternary regular mixing in the system, while the integral evaluates the free energy deviations due to short- and long-range ordering. The step in the λ parameter was set equal to 0.04. Steps in mole fractions and in the temperature were 0.03125 and 50 K, respectively; the temperature varied from 598 to 98 K. Isosurfaces of the Gibbs energy of mixing were computed over a grid of 561 ternary compositions.

2.1.6. Representation of the free energies of mixing

Obviously, the digital character of the obtained Gibbs energies poses a problem in applying them for calculating thermodynamic equilibrium in chemically complex systems. Indeed, the currently available software tools, e.g. GEM Selector (Kulik et al., 2013) require the Gibbs energy to be expressed as a differentiable function of the composition. This implies that the Gibbs free energy grid obtained from a Monte Carlo simulation must be fitted into a mathematically suitable form. In this study, this was achieved via the ternary regular mixing model, in which the enthalpy of mixing was modelled via Eqn. (13), while the interaction parameters were adjusted to the Monte Carlo results such that the shape of the ternary miscibility gap was closely reproduced. Although such a fit can be performed via an automatized routine, here it was performed via a manual variation of the binary W_{ij} parameters. Indeed, we noted that the shape of the miscibility gap in the ternary system is mostly sensitive to the value of W_{BaSr}. The optimal set W_{ij} values, which best fits the Monte Carlo results could be relatively easily found via a very limited set of regular model calculations consisting of two steps. At the first step, the value of W_{BaSr} was varied within the interval of 4–9 kJ/mol with a step of 0.05 kJ/mol, while the W_{BaRa} and W_{SrRa} were fixed at the values predicted via the SDM calculations. At the second step the values of W_{BaSr} and W_{BaRa} were fixed and the value of W_{SrRa} was varied. The ternary miscibility gap was visualized by constructing a convex hull and by projecting it onto the ternary composition diagram, as described by Vinograd et al. (2010). In the convex hull algorithm, each point of the original free energy surface is substituted by a combination of three points corresponding to the energies that give the lowest energy value for the same average composition. A concave area is thus substituted by a triangle of the minimal size that is defined by the grid density. Miscibility gaps can thus be visualized as agglomerations of large thin triangles elongated along tie-lines, while miscible regions are seen as agglomerations of isometric triangles of minimum area.

2.2. Celestite recrystallization in the presence of a Ra-bearing aqueous solution

2.2.1. Sample preparation and experimental setup

The general batch experimental setup was adapted from earlier studies on barite recrystallization (e.g. Brandt et al., 2015; Klinkenb[illegible] et al., 2014). A high purity celestite (99.99+ %), as p[illegible] Chempur®, was put into contact with a Ra[illegible] and the uptake of Ra wa[illegible] $5.0 \cdot 10^{-6}$ moL/L and 0.[illegible] Chempur® celestite is cl[illegible] between 0.5 and 5 µn[illegible] carried out in order to [illegible] from celestite in the p[illegible] addition, a blank exp[illegible] the adsorption of Ra [illegible] is given in Table 1.

Blank Ra			
Reference 0.5 g/L SrSO4_RT	0.5		
0.5 g/L SrSO4_RT	0.5	5	828

2.2.2. Sampling and analyses of the aqueous solution

The sampling procedure was the same as in Klinkenberg et al. (2014), i.e. 500 µL of the aqueous solution were taken at regular time intervals and directly filtered after a settling time of 1 h through Advantec ultrafilters (MWCO = 10,000 Da). The Ra concentration in solution was quantified via Gamma spectrometry using a N_2 cooled high purity Ge-detector. The intensity of the Ra peak at 186 keV was determined using Gamma-W for Windows (Version 2.55, Interaktive Spektrum Analyse, Dr. Westmeier, Gesellschaft für Kernspektrometrie mbH) and converted to a concentration (mol/L). The system was calibrated with an independent, external standard. The Sr and Ba concentrations in solution were quantified using an ICP-MS ELAN 6100 DRC (PerkinElmer SCIEX) instrument. The filtered solution was diluted in 0.1 m HNO_3.

2.2.3. Analysis of the solids: scanning electron microscopy (SEM) and energy dispersive x-ray spectrometry (EDS)

Small amounts of solid were sampled during the recrystallization experiments. The evolution of the crystals morphology and chemical composition was studied using the environmental scanning electron microscope FEI Quanta 200 FEG combined with energy dispersive x-ray spetcrometry (EDS, EDAX). In order to avoid artifacts due to precipitation of NaCl, $SrSO_4$ or $RaSO_4$, the samples were separated from their solution by two washing steps in iso-propanol. The samples were then prepared as a suspension on a Cu holder and subsequently dried.

2.3. GEM-selector thermodynamic modelling

SS-AS equilibria were modelled with the GEM-Selektor code package (Kulik et al., 2013; http://gems.web.psi.ch) that includes the TSolMod library of models of mixing (Wagner et al., 2012) and the GEMS version of PSI-Nagra 12/07 chemical thermodynamic database (Hummel et al., 2002; Thoenen et al., 2014). In GEM-Selektor, the phase equilibrium is found via direct minimization of the total G[illegible] energy of the system defined by its bulk elemental compos[illegible] perature, pressure, standard Gibbs energy per mol[illegible] species, and parameters of mixing in phases-sol[illegible] data for solid sulfates (Table 2) and for [illegible] the GEMS version of the PSI-Na[illegible] inherits temperature and [illegible] for most aqueou[illegible] water [illegible]

A complete thermodynamic dataset for the system (Ba,Sr,Ra)$SO_4 + H_2O$ in GEMS and PHREEQC forms that includes the temperature dependence of $RaSO_4$ solubility is discussed in a companion paper (Vinograd et al., 2017).

3. Results

3.1. Thermodynamics of mixing in the ternary system

3.1.1. Parameterization of the regular model of mixing

The results of calculations based on the single defect method (SDM) have been already reported for some of the binary systems within the barite family (Vinograd et al., 2013). In this study, these calculations are repeated with a better precision and the results are extended to all possible combinations of the host-solute pairs to give a complete set of the subregular model parameters for (Ba,Sr,Ra)SO_4 solid solution. Here we also demonstrate the consistency between values of regular mixing parameters computed with the single-defect method and those obtained with the aid of quasi-random structures (QRS). The binary $W_{IJ/J}$, $W_{IJ/I}$ and W_{IJ} parameters computed with the SDM are given in Tables 3 and 4. Table 3 gives the values computed with the DFT-based CASTEP code, while Table 4 lists the analogous values computed from the modified force-field model of Allan et al. (1993). Fig. 1 shows the enthalpy of mixing functions of the binary (Ba,Ra)SO_4, (Ba,Sr)SO_4 and (Sr,Ra)SO_4 systems computed ab initio with the SDM. The Sr-Ra and Ba-Ra binaries are characterized by the largest and the smallest enthalpies of mixing, respectively. This is consistent with the observation that the excess effect is proportional to the squared volume difference between the end-members (Vinograd et al., 2013; Kowalski and Li, 2016). The results obtained with quasi-random structures (QRS) are also shown in Fig. 1 and given in Table 3. Obviously, the enthalpies of the QRS are consistent with the SDM results. The differences between these two sets of values can be interpreted as the uncertainties of the derived parameters. This uncertainty does not include systematic errors inherent to the functional and the pseudopotentials used in the DFT calculations. We assume that the latter errors should not exceed the differences between the W values given in Tables 3 and 4 The total uncertainty is taken as the sum of the two differences. The SDM DFT-based average values are taken as the final result. The values $W_{BaRa} = 2.47 \pm 0.22$, $W_{BaSr} = 8.34 \pm 0.75$ and $W_{SrRa} = 19.80 \pm 1.40$ kJ/mol were used to compute the Gibbs free energy of the ternary regular solid solution (see Section 3.1.2).

3.1.2. Ternary regular model

Fig. 2 shows the convex-hull analysis of the Gibbs free energy surface which corresponds to the ternary regular model with the W_{ij} parameters from Table 3 (the average SDM values). The miscible convex areas are seen as agglomerations of small triangles, while the miscibility gaps appear as agglomerations of elongated trian

Table 3
Binary Margules parameters (
single-defect and QR structure

Subregular model (SDM)								
$W_{BaRa/Ba}$	2.63	W_{BaR}						
$W_{BaSr/Sr}$	7.75	W_{Ba}						
$W_{SrRa/Sr}$	20.31	W_{Sr}						
$W_{BaRa/Ra}$								
$W_{BaSr/Sr}$	9.01	$W_{BaSr/Ba}$	8.78	W_{BaSr}				
$W_{SrRa/Ra}$	19.29	$W_{SrRa/Sr}$	20.63	W_{SrRa}	19.96	W_{SrRa}	20.00	

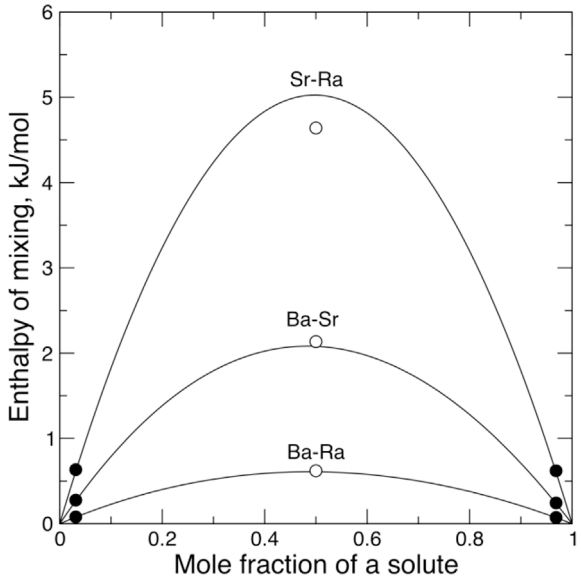

Fig. 1. Enthalpies of mixing in binary systems computed with the single defect method. Solid lines correspond to the subregular model, where the Margules parameters are given in Table 3. The solid circles in the dilute limits are the excess enthalpies of the single-defect supercell structures per one SO_4 unit. The open circles at intermediate compositions are the excess enthalpies of quasi-random structures scaled per one SO_4 unit.

Importantly, the elongations of these triangles approximately follow the tie-lines. The model predicts a large miscibility gap within the ternary. At ambient temperatures, the miscibility is restricted to two composition domains, the Ba,Ra-rich, Sr-poor phase, in which complete mixing is observed at all temperatures above 198 K, and the Sr,Ba-rich, Ra-poor phase, whose composition extends towards $BaSO_4$ at $T > 500$ K. In the (Ba,Sr)SO_4 binary, the miscibility gap closes at about 500 K, while in the (Sr,Ra)SO_4 system it is present up to ~1200 K. The predicted v
of W_{BaSr} of 8.3 kJ/mol that causes the gap closing above 500
to contradict to observations from natural samples (e
2014), which suggest that full miscibility exist
agenetic conditions (300 < T < 400
servation, Heberling et al. (201
range of Ba/Sr ratios in
pipes of a hydrot
a miscib

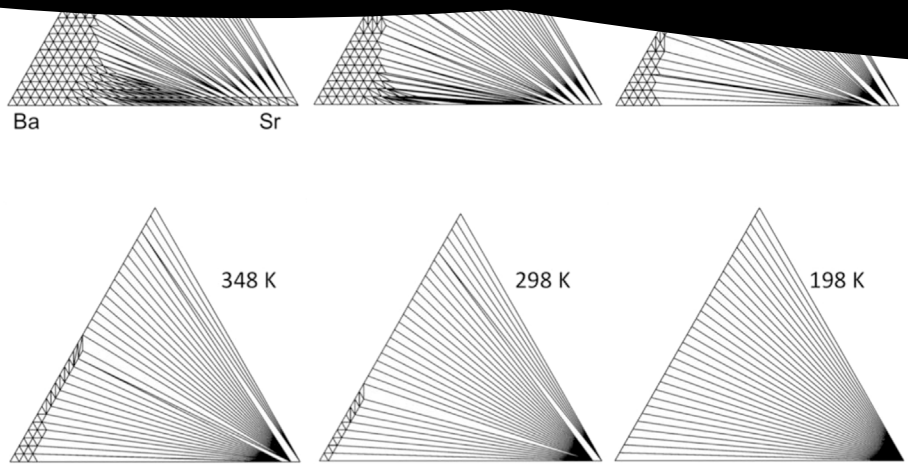

(right). The patterns of the energy change vs. distance are very similar in all three systems. The magnitude of the pairwise interactions increases consistently with the volume mismatch between end-members.

The effect of composition on the pairwise interactions was further investigated with DFT for (Ba,Ra)SO_4 and (Ba,Sr)SO_4 systems. Fig. 4 (left) compares the excess energies of RaRa defects in a barite host to the excess energies of BaBa defects in a $RaSO_4$ host. The insertion of RaRa pairs into the barite host causes slightly larger excess energies. This is consistent with the usually observed stronger increase in the energy upon an insertion of a larger cation, which is related to a more rapid increase of the interaction energy of two ions upon a contraction rather than on an extension (Dove, 1993). The patterns of energy change vs. the defect-defect separation are very similar in the two sets. This shows that BaRa interactions, i.e. the energies of reactions BaBa + RaRa = 2BaRa, are approximately independent of the composition of the binary system. The whole set of data on (Ba,Ra)SO_4 thus confirms the previous result (Vinograd et al., 2013) that the mixing in this system can be well described with a regular model with the W parameter in the range of 2.3–2.6 kJ/mol. The average value of 2.47 kJ/mol obtained from Ba and Ra defects in $RaSO_4$ and $BaSO_4$, respectively, is adopted for further modelling studies.

A rather different picture is seen in the case of BaSr interactions. The excess enthalpies of BaBa defects in the $SrSO_4$ host on average are smaller than the analogous values for SrSr defects in $BaSO_4$ (Fig. 4, right).

This observation is consistent with the SDM result (Table 3), which shows that the insertion of a single Ba^{2+} into $SrSO_4$ costs less energy that the insertion of a single Sr^{2+} into $BaSO_4$. This causes $W_{BaSr/Sr}$ to be smaller than $W_{BaSr/Ba}$. We note also that the excess energies of structures with BaBa defects placed at the third-, fifths- and sixths-neighbour distances are markedly smaller than the energies of the other structures (Fig. 4, right). These structures appeared to be not stable within the barite symmetry. A similar problem occurred with supercell structures containing RaRa defects in the celestite host. The origin of this anomalous behaviour is explained in Appendix A1. Therefore, in the present study, the BaSr and RaSr pairwise interactions were computed only from SrSr-defect structures built from the $BaSO_4$ and $RaSO_4$ hosts, respectively. The effects of composition on pairwise interactions were estimated based on the difference in the excess energies of the single-defect structures. Therefore, the values of $J_{BaSr/Sr}$ were scaled relative to the values of $J_{BaSr/Ba}$ by a factor of 0.87, while the values of $J_{SrRa/Sr}$ were scaled by a factor of 1.052 relative to the values of $J_{SrRa/Ra}$. This scaling ensured the consistency between DDM and SDM results. On the other hand, the absence of a strong asymmetry in binary W para

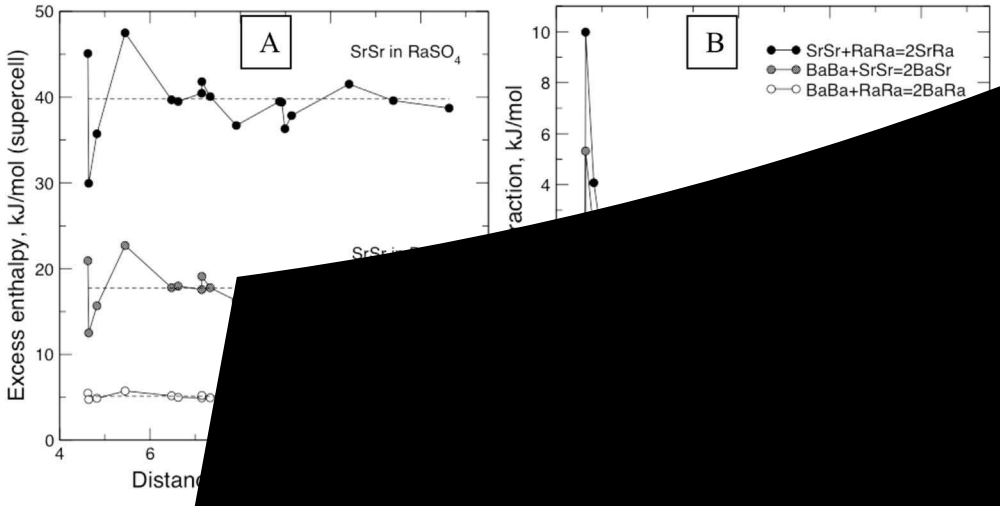

Fig. 3. Left: Excess en
percells of BaS
of pair

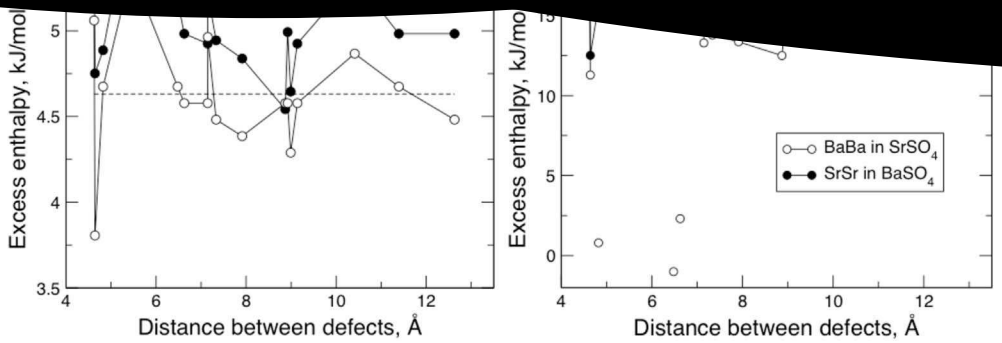

ergies are computed with DFT.

(Tables 3 and 4) justifies the assumption that there should be no strong asymmetry in the pairwise binary interactions. This implies that the DFT-based interaction energies, which are computed only for Ba-rich and Ra-rich compositions, could be used to model the whole ternary composition space. The set of the pairwise interactions is given in Appendix A3. These interactions were used to define the mixing energy in the ternary Monte Carlo Ising model.

3.1.4. The generalized Ising ternary model

Table A2 in Appendix A3 lists the pairwise interaction energies, which were used to simulate the ternary mixing. A distinction between the phase relations predicted based on the regular mixing and the generalized Ising model is primarily seen in the $(Ba,Sr)SO_4$ binary. In the generalized Ising model, the Ba-Sr miscibility gap occurs at a much lower temperature. Particularly, the regular model predicts the closing of the miscibility gap at about 500 K, while in the Ising model, the closing occurs at about 280 K. The stabilization of the disordered phase relative to the mixture of the end-members is due to short-range ordering (SRO). The SRO effect is best seen in the enthalpy vs. composition plot as a significant decrease in the enthalpy of mixing at ambient temperatures (Fig. 5). The systems of $(Ba,Ra)SO_4$ and $(Sr,Ra)SO_4$ are much less sensitive to a similar ordering. In the former case, the pairwise interactions are very weak. The phase separation occurs below 150 K, i.e. at the temperatures, which are not particularly interesting for the present study. At ambient temperatures, the solid solution is essentially disordered. In the case of $(Sr,Ra)SO_4$, on the contrary, the pairwise interactions are strong and their total excess effect is so large that the solid solution decomposes at all temperatures of interest. Thus, at ambient temperatures the solid solution exists in the dilute limits only, where the regular mixing model remains valid. This implies that the $(Ba,Ra)SO_4$ and the $(Sr,Ra)SO_4$ solid solutions can be adequately modelled via the regular mixing model, while a SRO correction is required only in the $(Ba,Sr)SO_4$ binary.

Fig. 6 shows the convex-hull analysis of the free energy surfaces computed via the thermodynamic integration of the Monte Carlo results.

The effect of the SRO on the free energy of the solid solution can be emulated with the help of the regular mixing model by decreasing the W_{BaSr} parameter to ~4.95 kJ/mol such that the miscibility gap closes at ~280 K as in the DDM-Monte-Carlo modelling. A small decrease in the W_{SrRa} parameter relative to the SDM value also helps to approach the shape of the ternary miscibility gap produced using the Ising model. Thus, the set of parameters (W_{BaRa} = 2.47 ± 0.22, W_{BaSr} = 4.95 ± 0.75 and W_{SrRa} = 17.50 ± 1.40 kJ/mol) together with the regular model equations can be used to emulate the phase relations computed with the rather tedious Monte Carlo simulations. Here, we would like to mention that the fit to the simulated ternary phase relations could be further improved, for example, by introducing asymmetry in the regular expressions for the binary systems. Our s
mistic simulations show, however, that mixing in the binary s
very close to be symmetric. Thus we decided not to
further complexities into the ternary model. Alth
that the regular description in principle c
complex shape of the free energy
over a wide temperatur
Margules paramet
298–398

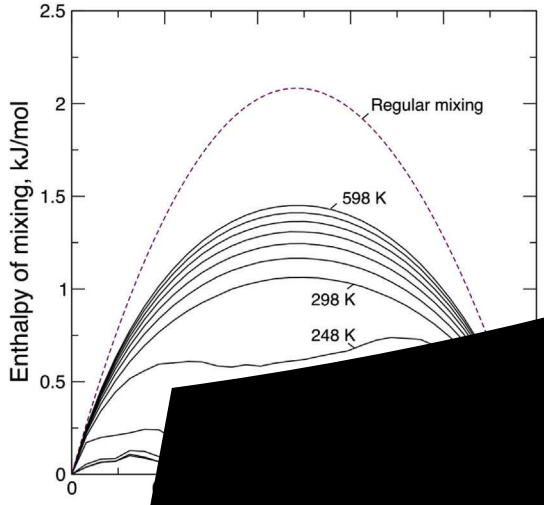

Fig. 5. The enthalpy of mi
the Monte Carlo method
parameters $W_{BaSr/Ba}$ = 8

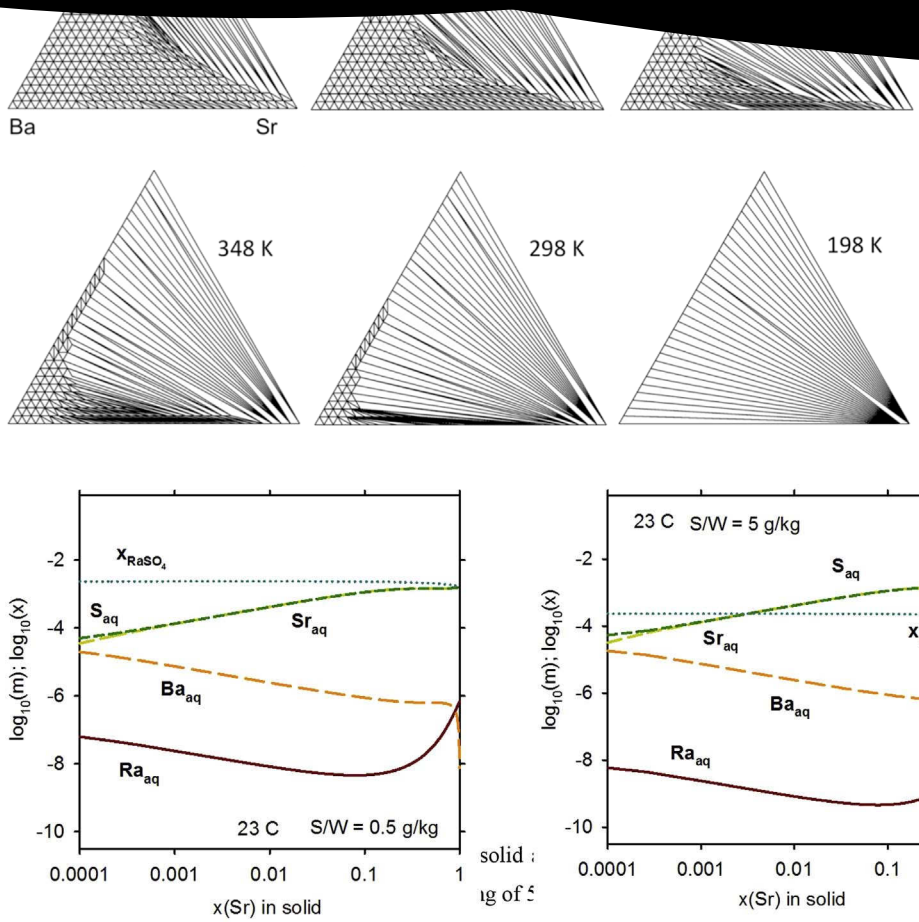

Fig. 7. Dependencies of the Ra contents in the solid and aqueous phases at 23 °C at 1 bar on the mole fraction of Sr in the solid phase at trace Ra loading of $5{\cdot}10^{-6}$ m and S/W = 0.5 (A) and 5.0 g/(kg H_2O) (B).

solution phase remained constant. The results of the simulations (Fig. 7) show that at Ba-rich compositions, the equilibrium aqueous concentration of Ra decreases as a function of the mole fraction of $SrSO_4$ in the solid, such that a clear minimum is observed at ~10 mol % $SrSO_4$.

This implies that the immobilization of Ra in the ternary (Ba,Sr,Ra)SO_4 solid solution at $x(SrSO_4) \sim 0.1$ is much more efficient than in the binary (Ba,Ra)SO_4 solid solution. On the other hand, at higher $x(SrSO_4)$, particularly above 0.5, the immobilization of trace Ra is predicted to be less efficient than in the (Ba,Ra)SO_4 solid solution. The retention of Ra in the solid is more efficient at the higher S/W of 5.0 g/(kg H_2O). Fig. 7 shows that Ra,aq concentrations are ca. 10 times higher at S/W = 0.5 g/(kg H_2O).

3.2.2. Modelling of the effect of Sr/Ba ratio on Ra uptake in the case of phase separation

Although at trace Ra-concentration, th
dicted to be completely
vated Ra-concentrations
ternary miscibility gap
$RaSO_4$ causes the solid
phase, which is simul
decomposition with
solutions (with identi
possible phases. The
system composition

of solid (Ba,Sr)SO_4 sulphate. With this total composition, the ternary solid solution becomes unstable at any composition above $x(SrSO_4) \sim 0.4$ (Fig. 8, left). At lower Sr/Ba ratios, the system behaviour is very similar to that described in the previous section, i.e. the aqueous Ra content goes through a minimum at about $x(SrSO_4) \sim 0.1$ and th
steadily increases. Although the concentrations of Ra, Ba and S
aqueous phase change continuously across the decompos
fractions of $BaSO_4$, $RaSO_4$ and $SrSO_4$ in the sol
dramatic changes at $x(SrSO_4) \sim 0.4$. Th
through a nucleation of a minor Ba
$(SrSO_4) < 0.75$ the Ba cont
content of Ba in th
content of R

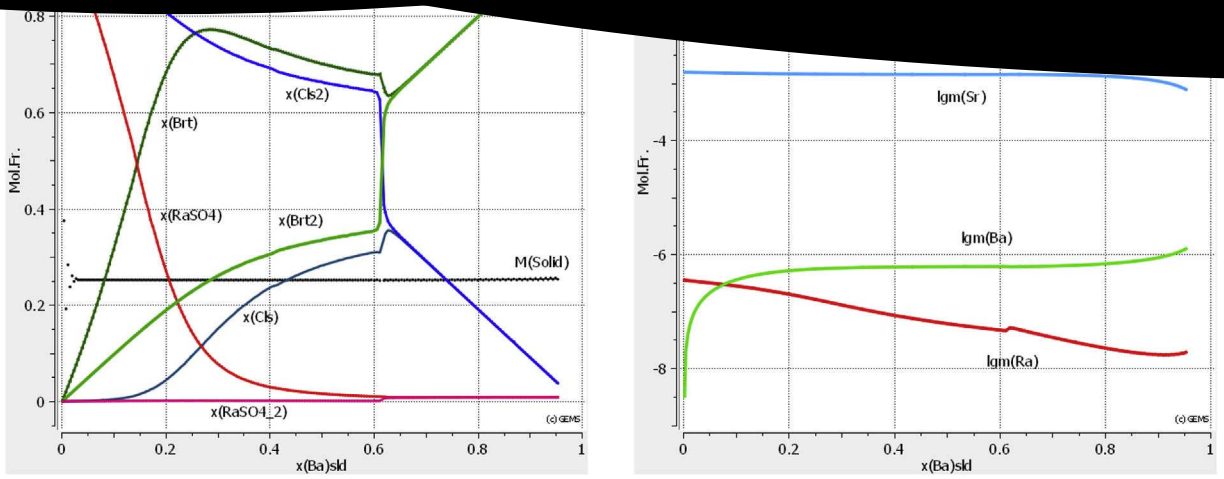

Fig. 8. Evolution of the composition of two ternary solid solutions Sulphate and Sulphate2 (A) and aqueous (B) phases as functions of the increase in the fraction of Ba in the system ar 23 °C, 1 bar. End members: Sulphate: Cls (celestite), Brt (barite), $RaSO_4$ (radium sulphate); Sulphate2: Cls2 (celestite), Brt2 (barite), $RaSO_4$_2 (radium sulphate). The system composition is defined by 1 kg of H_2O with $1{\cdot}10^{-5}$ mol/(kg H_2O) $RaCl_2$ and 0.25 g/(kg H_2O) of solid (Ba,Sr)SO_4 sulphate. The figure is generated with GEM-Selektor.

more than 90%. The radium uptake appears to be connected to the release of Ba from the solid phase, where it is present in minor/trace amounts. In the presence of radium, elevated concentrations of Ba in the aqueous solution are observed, especially at the beginning of the experiment. At day 1, the aqueous Ba concentration in the Ra-containing celestite recrystallization experiment is almost one order of magnitude higher than in the Ra-free reference experiment. During the experiment, in the presence of Ra, the Ba-concentration decreases, but stays higher by a factor of ~4 compared to the Ra-free experiment, even after 828 days. Between day 226 and day 828, the concentrations of Ra, Ba and Sr in solution practically stop changing, indicating an approach to a steady state or to the equilibrium.

3.3.2. Scanning electron microscopy of the equilibrated celestite

Already at day 1, tiny idiomorphic crystals on the surface of celestite were seen, which appeared brighter in the back-scattered electron (BSE) image. If it were not for the difference in the brightness, these crystals could be easily missed in the BSE investigation. EDS analyses carried out on these crystals have shown clear peaks of Ra and Ba peaks (Fig. 10). A Ra:Ba ratio of 1:2 was typical for all analyses taken after 226 and 828 days (Table 5). These Ra-rich crystals remained present for more than 800 days (Fig. 10). On the contrary, no Ba-rich crystals were detected in the reference experiments without Ra with the same celestite sample.

4. Discussion

Our study provides a detailed description of the mixing properties of the ternary solid solution, which includes effects of short-range ordering. This description is based on an extensive set of ab initio calculations on supercells with single and paired substitution defects. A question is, whether this effort provided a model, which can ultimately be trusted. We argue here that our results for the sulphate solid solutions appear to be very reasonable. The set of binary *W* parameters is consistent with the observation that the main effect of non-ideality in the studied systems is determined by the size mismatch between the exchangeable cations, which is proportional to the squared volum mismatch between the end-members (Vinograd et al., 2013; K and Li, 2016). The magnitudes of pairwise ordering inter the same proportionality. The strongest pairwise in

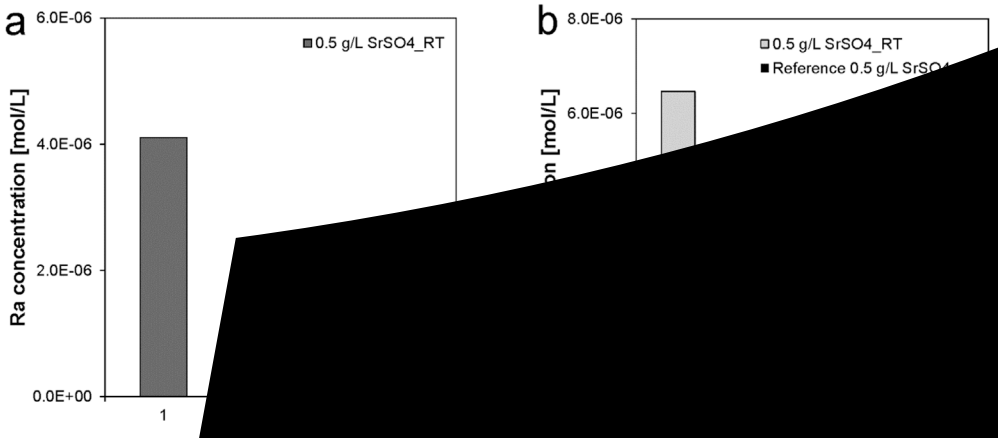

Fig. 9. Te

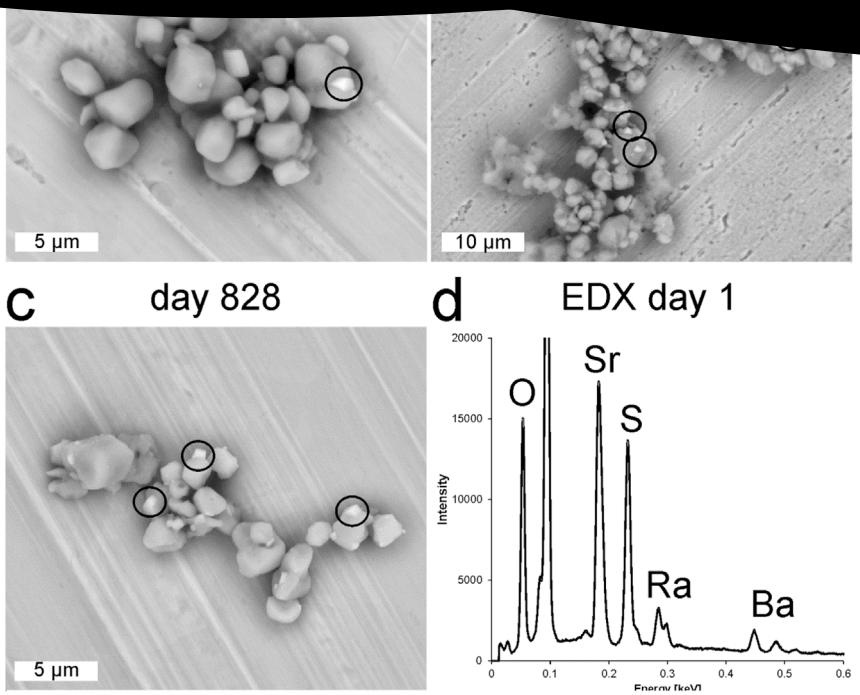

Table 5
Results of EDX determination of the Ra/Ba ratios of the tiny Ra-rich crystals.

Day	Ra	Ba	Ra/Ba	Ra/Ba
	[at%]	[at%]		mean value
1	1.01	1.22	0.83	
226	1.28	2.26	0.57	
	0.48	0.97	0.49	
	0.78	2.01	0.39	
	0.74	2.00	0.37	0.45
828	1.01	1.95	0.52	
	2.38	5.47	0.44	
	1.38	2.64	0.52	
	0.97	1.76	0.55	
	1.54	3.34	0.46	0.50

between Ra and Sr, while the weakest are those between Ba and Ra. Although the ordering interactions are very strong in $(Ra,Sr)SO_4$, we claim that both $(Ra,Sr)SO_4$ and $(Ba,Ra)SO_4$ systems at ambient temperatures can be well described via the regular mixing model, while a special treatment based on the generalized Ising model is required only for Ba-Sr interactions, which are of intermediate strength. The re
that in the $(Ra,Sr)SO_4$ system, the overall effect of
actions causes a wide miscibility
the miscibility still exist
ture. In the $(Ba,Ra)SO_4$
that a significant SRO
higher temperatures, t
ular model. On the co
system are strong eno
most relevant temper
plays an important

binary and in the ternary system. Our results suggest that the critical miscibility is the $(Ba,Sr)SO_4$ solid solution occurs at about 280 K. Thus, at repository conditions, we expect this solution to be fully miscible. This model is fully consistent with the wide range of barite and celestite compositions observed in Opalinus Clay formation, which experienced diagenetic conditions with temperatures about 350 K (Lerouge et al., 2014).

This model, together with the standard thermodynamic data of Ba, Sr- and Ra-sulphates and relevant aqueous species available in the PSI-Nagra database (Thoenen et al., 2014), allows an investigation of the effect of Sr in barite on Ra-uptake. Our GEM-Selektor simulations at ambient temperatures predict that Ba-Sr sulfates with intermediate Sr/(Ba + Sr) ratios are more efficient (by a factor of 7-8) for Ra-uptak
compared to the case of Sr-free $BaSO_4$ barite. Our simulation
under the assumption of reasonably large S/W ratios, sh
rocks containing celestites with less than 90% of Sr
as very efficient Ra absorbers. Equilibrium
pore water would be quite low du
activity in the aqueous phas
sulfates.

An inter
sh

dicted phase separation in the ternary solid solution. The observed nucleation of Ba- and Ra-rich crystals on the celestite matrix in the case of the Ra addition to the system, and the absence of such a nucleation in Ra-free experiments, corroborates the concept of phase separation, which, at high Sr/Ba ratios, requires a coexistence of Ba-Ra-rich solid solution with an almost pure celestite. Particularly interesting is the experimental observation of an increase in the Ba content of the aqueous phase upon the addition of $RaBr_2$. When no $RaBr_2$ is added, Ba happily resides within the $SrSO_4$ phase in a form of a dilute solid solution. Due to the dilution, the activity of Ba in the aqueous phase is kept very low. However, as soon as a new Ba- and Ra-rich phase is formed, the dilution effect is greatly diminished, and the aqueous content of Ba elevates significantly. This effect is observed both in our experiments and in thermodynamic simulations (Fig. 8).

On the other hand, we note that only a partial equilibrium has been achieved in our experiments. Our simulations show that the measured Ra/Ba ratio of 0.5 would require a much higher Ba/Sr ratio in the system, if the complete equilibration were assumed. Indeed, the mole fraction of $RaSO_4$ of ~1/3 in the minor phase would require x(Ba) ~0.2 in the newly-formed solid shown on Fig. 8. Apparently, a large fraction of celestite remained "dormant" during the equilibration. We assume that soon after the Ra–containing aqueous solution was brought into a contact with 0.5 g/L celestite, about of 60% of the solid was dissolved. This initial dissolution provided the aqueous solution with a sufficient amount of Ba,aq and SO_4,aq to cause the precipitation of a $(Ba,Ra)SO_4$ phase and of a certain amount of Sr-rich $(Sr,Ba)SO_4$ phase. The latter phase presumably remained undetected due to its similar SEM contrast with the bulk (unreacted) celestite. Further evolution of the system involved a gradual re-equilibration of the $(Ba,Ra)SO_4$ and $(Sr,Ba)SO_4$ phases with the initial mass of the celestite. This evolution led to an increase in the Sr-content of $(Sr,Ba)SO_4$ phase and, consequently, to a decrease in the Ra content of the $(Ba,Ra)SO_4$ phase. Indeed, the Ra/Ba ratio appears to be slightly smaller in Ra-rich crystals equilibrated for longer time intervals (Table 5). An important observation is that the tiny Ba- and Ra-rich crystals remained stable within the whole experimental time interval of 828 days. This is an indication that the phase relations in the system are governed by the ternary miscibility gap.

The observed nucleation of a Ra- and Ba-rich phase upon the interaction of a Ra-bearing solid solution with celestite has two important implications. First, our simulations and experimental results suggest a synthesis route with which very Ra-rich crystals can be crystallized from aqueous solution at a reasonably low total Ra activity. Thus, there could appear a possibility to measure certain physical properties of these crystals. Second, the predicted formation of Ra-rich crystals at high Sr/Ba ratios implies that in such systems, the dilution effect loses its important role as a factor of Ra-retention.

5. Conclusions

Our study provides a set of interactio

Appendix

A1. Consequences of ins

Visual analysis of t
that they adopted a r
structure. The regula
composition of Sr_{32}(

especially important in the (
dicts complete mixing in the Ba-Ra and Ba-Sr binaries at and above 25 °C and a large miscibility gap in the Ra-Sr binary. This gap significantly expands into the ternary composition space.

GEM-Selektor calculations of equilibria in the $(Ba,Sr,Ra)SO_4$ SS-AS systems show that, in agreement with previous experimental and theoretical studies, an increase in the host solid-water mass ratio is always a positive factor for Ra uptake. An important prediction made in the present study is that a moderate increase in the Sr/Ba ratio leads to an even stronger Ra retention: the presence of $SrSO_4$ in the solid solution up to 5–10 mol % reduces the dissolved Ra,aq concentration by factor of 7–8 compared to the previously studied SS-AS systems containing no $SrSO_4$ (e. g. Bosbach et al., 2010; Curti et al., 2010; Klinkenberg et al., 2014; Brandt et al., 2015). However, a further increase in the Sr/Ba ratio makes Ra retention less effective. The latter effect has been modelled in SS-AS systems both with and without phase separation. In systems with low Ra loading, there is a complete mixing within the ternary solid phase, $(Ba,Sr,Ra)SO_4$, containing a trace amount or $RaSO_4$. In this case, the uptake of Ra into the solid decreases due to the dependence of $\gamma(RaSO_4)$ on W_{SrRa}. On the other hand, in systems, in which the fraction of $SrSO_4$ is close to one, a minor amount of $RaSO_4$ causes a phase separation. A phase, which is simultaneously rich in Ba and Ra then coexists with a nearly pure celestite. The Ra/Ba ratio in the barium-rich phase increases with the increase of the Sr/Ba ratio in the system. In such a system, a reduction in Ra-retention is primarily caused by an increase in the mole fraction of $RaSO_4$ $x(RaSO_4)$, which makes the dilution effect less effective.

The results of the present study significantly improve our understanding of efficiencies of natural types of barite in Ra retention. These results benefited from new atomistic approaches to study the thermodynamics of mixing in solid solutions, which are, in turn, based on the recent progress in first-principles calculations, and from the use of advanced Gibbs energy minimization algorithms, adapted to ternary mixtures, as implemented within the GEM-Selektor package (http://gems.web.psi.ch). The ultimate validation of our results has been provided by a direct experimental study of Ra-uptake, which required precise measurements on samples with rather high radioactivity.

Acknowledgements

The research leading to these results ha
from the German Federal Ministry of
(joint projects ImmoRad (gr
02NUK039)) and from
VI-196/2-1 a

did not show any sign of the monoclinic distortion on relaxation. This
parameters, which are consistent with the orthorhombic symmetry.

The relative stabilities of the $P2_1/n$ and Pnma forms of $SrSO_4$ were also investigated with the modified force-field model of Allan et al. (1993). Contrary to the DFT calculations, the force-field calculations predicted the $P2_1/n$ form to be less stable than the orthorhombic one. Even when the force-field geometry optimization starts from the $P2_1/n$ structure, the final result is the Pnma barite. The predicted metastability of the Pnma $SrSO_4$ requires a further investigation. Possibly, it occurs just within the adopted DFT computational scheme. Since we were interested in the mixing properties of the solid solution relative to barite-type endmembers, the supercell structures that reflected the stability of the $P2_1/n$ structure were excluded from any further analysis. Consequently, the present analysis of mixing effects in the $(Ba,Sr)SO_4$ binary is based only on the supercell structures with SrSr defects in $BaSO_4$. The same problem prevented the computation of the barite-type pairwise interactions from the structures with RaRa defects in $SrSO_4$.

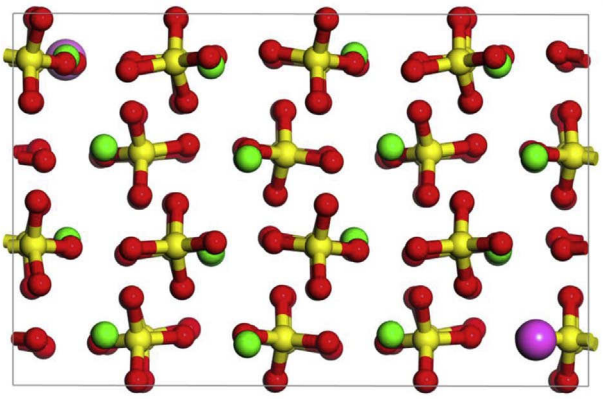

Fig. A1. Converged geometry of a $2 \times 2 \times 2$ supercell of celestite with a pair of Ba defects (pink spheres) at the third distance ($n = 3$) in the projection onto the *a*-*b* plane. Note the regular pattern of rotations of the SO_4 tetrahedra. This pattern is consistent with a monoclinic structure of $SrSO_4$.

A2. The ternary interaction parameter

In this study, a special care was taken to estimate the value of the ternary interaction parameter in Eqn. (13). Based on the cation size argument, one could assume that an admixture of Ba^{2+} to the equal mixture of Sr^{2+} and Ra^{2+} would cost less energy than it is predicted with the ternary regular model, because the size of Ba^{2+} is almost equal to the average of the sizes of Sr^{2+} and Ra^{2+}. This argument would suggest that W_{BaSrRa} could be negative. To test this hypothesis, a set of 21 ternary quasi-random structures was simulated, and their excess enthalpies were computed with the force-field method. Fig. A2 shows the correlation between the enthalpy of mixing computed directly via the static energy minimization with GULP and the enthalpy predicted with Eqn. (13) with $W_{IJK} = 0$. Two models were tested. In the first case, the average W_{IJ} parameters were used as required by the regular mixing, while in the second case, the subregular behaviour was assumed in the binaries. Each ternary composition was represented either by 3 or 6 different QRS, and their average enthalpies were plotted. The observed linear correlations imply that the enthalpy of ternary mixing is accurately predicted via Eqn. (13) under the assumption that the interaction parameter is zero. If the ternary interactions were present, it would be impossible to match the enthalpies of ternary quasi-random structures via Eqn. (13) and $W_{\mathrm{BaSrRa}} = 0$.

Rigorously, these results only show that no ternary interaction parameter is required in the force-field model of the ternary mixture. I
good match between the binary *W* parameters computed from DFT and the force-field model together with the apparent linear
the both sets of these parameters and the relative squared volume difference of the endmembers (Vinograd et al., 2012)
energies are primarily of elastic origin and the force-field model should be sufficiently robust in the description of
we could be reasonably confident that a specific ternary interaction parameter is not needed. Fig. A2 sh
almost no advantage relative to the regular one. This is the consequence of the similarity betwee
studied here. Practically, this means that the subregular ternary model for (Ba,Sr,Ra)SO
regular one.

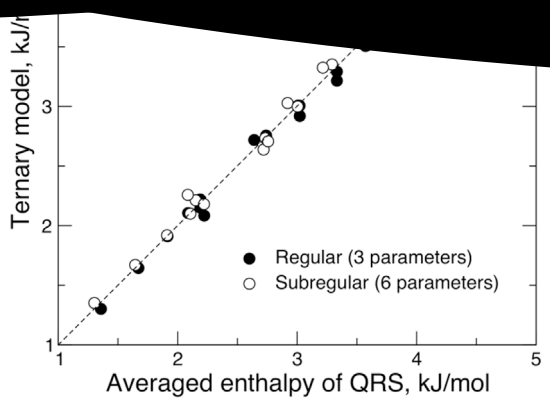

Fig. A2. The enthalpy of mixing in the ternary regular (subregular) solid solution parameterized via the Margules parameters of the binary systems vs. the excess enthalpy of a quasi-random structure.

A3 Parameters of the generalized Ising model for ternary sulphates

Table A1
Degeneracy numbers and coordination numbers in a $2 \times 2 \times 2$ supercell as a function of the order of neighbors.

n	D_n	Z_n
1	1	2
2	1	4
3	1	2
4	2	2
5	1	2
6	1	2
7	2	4
8	2	2
9	1	2
10	1	2
11	2	2
12	1	4
13	4	4
14	2	4
15	4	4
16	4	4
17	8	8

Table A2
The pairwise interactions derived from DFT calculations and used in Monte Carlo simul

BaBa + SrSr = 2BaSr:	
n	d(Å)
1	
2	
3	
4	
5	
6	
7	
8	

15	10.410	−0.19937		
16	11.393	−0.19198		
17	12.629	0.07775	0.06821	0.07299

BaBa + RaRa = 2BaRa:

n	*d*(Å)	$J_{BaRa/Ba}$	$J_{BaRa/Ra}$	$J_{BaRa/Sr}$
1	4.624	−0.32100	−0.38114	−0.35550
2	4.643	0.40871	0.89917	0.65394
3	4.824	0.27083	0.01280	0.14182
4	5.450	−0.29792	−0.33830	−0.31811
5	6.479	−0.02462	0.01280	−0.00591
6	6.626	0.17235	0.11129	0.14182
7	7.147	0.11572	0.05564	0.08568
8	7.150	−0.03201	−0.14133	−0.08667
9	7.335	0.21174	0.20978	0.21076
10	7.912	0.32008	0.30826	0.31417
11	8.870	0.31116	0.05564	0.18340
12	8.922	0.16250	0.11129	0.13689
13	8.990	0.12926	0.10169	0.11547
14	9.138	0.11572	0.05564	0.08568
15	10.410	−0.04063	−0.04604	−0.04333
16	11.393	0.04309	0.00320	0.02314
17	12.629	0.02154	0.02622	0.02388

SrSr + RaRa = 2SrRa:

n	*d*(Å)	$J_{SrRa/Sr}$	$J_{SrRa/Ra}$	$J_{SrRa/Ba}$
1	4.624	−5.15053	−5.25729	−5.20391
2	4.643	9.56539	9.76367	9.66453
3	4.824	3.94147	4.02317	3.98232
4	5.450	−3.74691	−3.82458	−3.78575
5	6.479	0.09846	0.10050	0.09948
6	6.626	0.28593	0.29185	0.28889
7	7.147	−0.32570	−0.33245	−0.32907
8	7.150	−0.98182	−1.00217	−0.99200
9	7.335	−0.27646	−0.28220	−0.27933
10	7.912	3.00415	3.06642	3.03529
11	8.870	0.14296	0.14593	0.14445
12	8.922	0.37966	0.38753	0.38
13	8.990	0.84477	0.86228	
14	9.138	0.93969	0.95916	
15	10.410	−0.42061	−0.42933	
16	11.393	0.04805	0.04904	
17	12.629	0.12947	0.1	

References

Allan, N.L., Rohl, A.L., Gay, D.H., Cat
Calculated bulk and surfa
Becker, U., Fernández-Gonzál
calculations of thermody
molecular principles. Ph
Bosbach, D., Boettle, M., Me
BaSO4 Kinetics of Solid
Reprecipitation. Tech
Swedish Nuclear Fuel
Brandt, F., Curti, E., Klinke
by a (Ba,Ra)SO_4 solid

°C. C.R. Acad. Sci. Ser. II 308, 1363–1368.
Ganguly, J., 2001. Thermodynamic modeling of solid solutions. In: In: Geiger, ChA. (Ed.), Solid Solutions in Silicate and Oxide Systems. EMU Notes in Mineralogy, vol. 3. EÖTVÖS University Press, Budapest, pp. 37–69 (Chapter 3).
Grandia, F., Merino, J., Bruno, J., 2008. Technical Report TR- 08–07: Assessment of the Radium–barium Co-precipitation and its Potential Influence on the Solubility of Ra in the Near-field. Svensk Kärnbränsle-hantering AB. Swedish Nuclear Fuel and Waste Management Company, Sweden.
Hanor, J.S., 2000. Barite-celestine geochemistry and environments of formation. In: Alpers, C.N., Jambor, J.L., Nordstrom, D.K. (Eds.), Reviews in Mineralogy. Sulfate Minerals, vol 40. Mineralogical Society of America, pp. 193–276.
Helgeson, H.C., Kirkham, D.H., Flowers, G.C., 1981. Theoretical prediction of the thermodynamic behavior of aqueous electrolytes at high pressures and temperatures: IV. Calculation of activity coefficients, osmotic coefficients and apparent and standard and relative partial molal properties to 600 _C and 5 kb. Am. J. Sci. 281, 1249–1516.
Heberling, F., Schild, D., Degering, D., Schäfer, T., 2017. How well suited are current thermodynamic models to predict or interpret the composition of (Ba,Sr)SO_4 solid-solutions in geothermal scalings? Geotherm. Energy 5, 9. http://dx.doi.org/10.1186/s40517-017-0068-x.
Hildebrand, J.H., 1929. Solubility, XII. Regular solutions. J. Am. Chem. Soc. 51, 66–80.
Hoshino, T., Schweika, W., Zeller, R., Dederichs, P.H., 1993. Impurity–impurity interactions in Cu, Ni, Ag, and Pd. Phys. Rev. B 47, 5106–5117.
Hummel, W., Berner, U., Curti, E., Pearson, F.J., Thoenen, T., 2002. Nagra/PSI Chemical Thermodynamic Data Base 01/01. Nagra technical report 02–16. .
Jacobsen, S.D., Smyth, J.R., Swope, R.J., Downs, R.T., 1998. Rigid-body character of the SO_4 groups in celestine, anglesite and barite. Can. Mineral. 36, 1053–1060.
Johnson, J.W., Oelkers, E.H., Helgeson, H.C., 1992. SUPCRT92: a software package for calculating the standard molal thermodynamic properties of minerals, gases, aqueous species, and reactions from 1 to 5000 bar and 0 to 1000°C. Comp. Geosci. 18, 899–947.
Klinkenberg, M., Brandt, F., Breuer, U., Bosbach, D., 2014. Uptake of Ra during the recrystallization of barite: a microscopic and time of flight-secondary ion mass spectrometry study. Environ. Sci. Technol. 48, 6620–6627.
Kowalski, P.M., Li, Y., 2016. Relationship between the thermodynamic excess properties of mixing and the elastic moduli in the monazite-type ceramics. J. Eur. Ceram. Soc. 36, 2093–2096.
Kulik, D.A., Berner, U., Curti, E., March 2004. Modelling chemical equilibrium partitioning with the GEMS-PSI code. In: Smith, B., Gschwend, B. (Eds.), PSI Scientific Report 2003/Volume IV, Nuclear Energy and Safety. Paul Scherrer Institute, Villigen, Switzerland, pp. 109–122 (ISSN 1423-7334).
Kulik, D.A., Wagner, T., Dmytrieva, S.V., Kosakowski, G., Hingerl, F.F., Chudnenko, K.V., Berner, U., 2013. GEMSelektor geochemical modeling package: revised algorithm and GEMS3K numerical kernel for coupled simulation codes. Comput. Geosci. 17, 1–24.
Lerouge, C., Grangeon, S., Gaucher, E.C., Tournassat, C., Agrinier, P., Guerrot, C., Widory, D., Flehoc, C., Wille, G., Ramboz, C., Vinsot, A., Buschaert, S., 2011. Mineralogical and isotopic record of biotic and abiotic diagenesis of the Callovian-Oxfordial clayey formation of Bure (France). Geochem. Cosmochem. Acta 75, 2633–2663.
Lerouge, C., Grangeon, S., Claret, F., Gaucher, E.C., Blanc, Ph, Guerrot, C., Flehoc, Chr, Wille, G., Mazurek, M., 2014. Mineralogical and isotopic record of diagenesis from the Opalinus Clay formation at Benken, Switzerland: implications for the modeling of
NAGRA, December 19[illegible]. Resistance of the High-level Waste Containers Proposed by NAGRA. The [illegible] Working Group on Container Technology.
NAGRA, 2014. Technischer bericht NTW 14-03. Charakt. Dosisintervalle Unterlagen zur Bewert. Barrierensysteme 1–61 ISSN 1015–2636.
Prieto, M., Heberling, F., Rodríguez-Galán, R.M., Brandt, F., 2016. Crystallization behavior of solid solutions from aqueous solutions: an environmental perspective. Prog. Cryst. Growth Charact. Mater. 62, 29–68.
SKB, 2011. Technical Report TR-11-01. Long-term safety for the final repository for spent nuclear fuel at Forsmark. Main report of the SR-Site project Volume III. Sven. Kärnbränslehantering Ab. 563–893 March 2011. ISSN 1404–0344.
Sluiter, M.H.F., Kawazoe, Y., 2002. Prediction of mixing enthalpy of alloys. Europhys. Lett. 57, 526–532.
Thoenen, T., Hummel, W., Berner, U., Curti, E., 2014. The PSI/Nagra Chemical Thermodynamic Database 12/07. PSI Bericht Nr. 14-04. ISSN 1019–0643.
Vinograd, V.L., Sluiter, M.H.F., Winkler, B., 2009. Subsolidus phase relations in the $CaCO_3$-$MgCO_3$ system predicted from the excess enthalpies of supercell structures with single and double de-fects. Phys. Rev. B 79, 104209.
Vinograd, V.L., Paulsen, N., Winkler, B., van de Walle, A., 2010. Thermodynamics of mixing in the ternary rhombohedral carbonate solid solution $(Ca_xMg_yMn_{1-x-y})CO_3$ from atomistic simulations. CALPHAD 34, 113–119.
Vinograd, V.L., Brandt, F., Rozov, K., Klinkenberg, M., Refson, K., Winkler, B., Bosbach, D., 2013. Solid–aqueous equilibrium in the $BaSO_4$–$RaSO_4$–H_2O system: first-principles calculations and a thermodynamic assessment. Geochim. Cosmochim. Acta 122, 398–417.
Vinograd, V.L., Kulik, D.A., Brandt, F., Klinkenberg, M., Winkler, B., Bosbach, D., 2017. Thermodynamics of the solid solution - aqueous solution system (Ba,Sr,Ra)SO_4 + H_2O: II. Radium retention in barite-type minerals at elevated temperatures. Appl. Geochem. http://dx.doi.org/10.1016/j.apgeochem.2017.10.019. Online: 20-NOV-2017.
Wagner, T., Kulik, D.A., Hingerl, F.F., Dmytrieva, S.V., 2012. GEM-Selektor geochemical modeling package: TSolMod library and data interface for multicomponent phase models. Can. Mineral. 50, 1173–1195.
Warren, M.C., Dove, M.T., Myers, E.R., Bosenick, A., Palin, E.J., Sainz-Diaz, C.I., Guiton, B.S., Redfern, S.A.T., 2001. Monte Carlo methods for the study of cation ordering in minerals. Mineral. Mag. 65, 221–248.
Weber, J., Barthel, J., Klinkenberg, M., Bosbach, D., Kruth, M., Brandt, F., 2017. Retention of ^{226}Ra by Barite: the Role of Internal Porosity. (accepted for publication in Chemical Geology).
Weigel, F., Trinkl, A., 1973. Crystalline chemistry of radium. 5. Diverse radium salts of inorganic anions. Radiochim. Acta 19, 199–202.
Wohl, K., 1946. Thermodynamic evaluation of binary and ternary liquid systems. Trans. Am. Inst. Chem. Eng. 42, 215–249.
Wu, Z.G., Cohen, R.E., 2006. More accurate generalized gradient approximation for solids. Phys. Rev. B 73, 235116.
Zhu, C., 2004. Coprecipitation in the Barite isostructural family: 1. Binary mixing properties. Geochim. Cosmochim. Acta 68, 3327–3337.
Zunger, A., Wei, S., Ferreira, L.G., Bernard, J.E., 1990. Special quasirandom structures. Phys. Rev. Lett. 65 (3), 353–356.